JOURNAL OF SPACECRAFT AND ROCKETS
Vol. 44, No. 4, July–August 2007

Solar-Sail Attitude Control Design for a Sail Flight Validation Mission

Bong Wie*
Arizona State University, Tempe, Arizona 85287-6106
and
David Murphy†
ATK Space Systems, Goleta, California 93117

DOI: 10.2514/1.22996

This paper presents the solar-sail attitude control system design for a solar-sail flight validation mission proposed in a dawn–dusk sun-synchronous orbit. The proposed solar-sail attitude control system architecture consists of a propellantless primary attitude control system and a microthruster-based secondary attitude control system. The primary attitude control system employs two ballast masses running along mast lanyards for pitch/yaw trim control and roll stabilizer bars at the mast tips for roll control. The secondary attitude control system uses lightweight pulsed plasma thruster modules mounted at the mast tips. Such a microthruster-based secondary attitude control system can be employed for attitude recovery maneuvers from various off-nominal conditions, including tumbling, that cannot be handled by the propellantless primary attitude control system. The overall simplicity, effectiveness, and robustness of the proposed solar-sail attitude control system architecture are demonstrated for a sail flight validation mission employing a 40-m, 150-kg sailcraft in a 1600-km dawn–dusk sun-synchronous orbit. The proposed solar-sail attitude control system will be applicable with minimal modifications to a wide range of future solar-sailing missions with varying requirements and mission complexity.

I. Introduction

THE recent advances in lightweight deployable booms, ultralightweight sail films, and small satellite technologies are spurring a renewed interest in solar sailing and the missions it enables. As a result, near-term solar-sail missions are being developed and the associated sailcraft technologies are rapidly progressing [1–4]. Solar sails have the potential to provide cost-effective, propellantless propulsion that enables longer mission lifetimes, increased scientific payload mass fraction, and access to previously inaccessible orbits (e.g., non-Keplerian, high solar latitudes, etc.). The solar-sail propulsion project of NASA's In-Space Propulsion program has been focusing on the quantitative demonstration of scalability of current solar-sail system architectures to future mission requirements through ground testing of key hardware systems [2–4]. In April 2005, Alliant Techsystems (ATK) and NASA successfully deployed a 20-m solar-sail as shown in Fig. 1 in the 30-m thermal vacuum chamber at the Plum Brook Space Power Facility of the NASA John H. Glenn Research Center [4]. However, development of a larger, flight-qualified solar sail as well as a solar-sail attitude control system (ACS) needs to be rapidly advanced so that a solar-sail spaceflight experiment for validating the principle of solar sailing, sail packaging and deployment, sail attitude stability and controllability, and sail thrust vector steering/pointing performance can be conducted in the near future.

Attitude stabilization of a fully deployed sailcraft by a conventional ACS of typical small spacecraft is not a viable option. Small reaction wheels and a conventional propulsion subsystem of a typical 100-kg class bus are unsuitable and/or inefficient for a fully deployed sailcraft because of its large moment of inertia and its large solar-radiation-pressure (SRP) disturbance torque. For example, a 40×40 m sailcraft with a nominal solar thrust force of 10 mN and a center of mass to center of pressure (cm/cp) offset of ± 0.1 m has an SRP disturbance torque of ± 1 mN $\cdot$ m, which is about 100 times larger than that of large geosynchronous communications satellites. A conventional ACS would require large reaction wheels and/or a prohibitively large amount of propellant to counter such a major disturbance torque acting on a large sailcraft for extended mission lifetimes. Most conventional control systems of small satellites can generate sufficient control torques for solar-sail applications, but their momentum storage and total impulse capabilities are unsuitable for most solar-sail applications. Consequently, propellantless attitude stabilization is required for most solar-sailing missions [5–7].

One method of properly maintaining the attitude of a large sailcraft against the solar disturbance torque is to employ small reflective control vanes mounted at the spar tips. Another method is to change the center-of-mass location relative to its center-of-pressure location. This can be achieved by articulating a control boom with a tip-mounted payload/bus. In [7], various dynamical models and attitude control systems of solar sails, using passive stabilization, spin stabilization, a two-axis gimbaled control boom, or translating/tilting sail panels, were developed. A sailcraft with three attachment points, as shown in Fig. 1, allows in-plane translation and rotation of four individual triangular sail panels, and thus it provides an ACS option for the propellantless, three-axis control with redundancy. Another option is to combine a two-axis gimbaled control boom for pitch/yaw control and roll stabilizer (spreader) bars for roll control for a propellantless three-axis control system.

Although the essential idea behind all these cm/cp methods appears simple, there are challenging hardware mechanization problems. Furthermore, all practical spacecraft control designs are often subjected to the physical limits of actuators, sensors, spacecraft structural rigidity, and other mission constraints. In particular, when a gimbaled control boom and/or sail control vanes are to be employed as primary actuators for active three-axis attitude control of solar-sail spacecraft, there exist a variety of practical issues, such as gimbal

Presented as Paper 5010 at the AIAA Guidance, Navigation, and Control Conference, Providence, RI, 16–19 August 2004; received 5 February 2006; revision received 11 December 2006; accepted for publication 18 December 2006.

*Professor, Department of Mechanical & Aerospace Engineering; currently Vance Coffman Endowed Chair Professor, Department of Aerospace Engineering, Iowa State University, 2271 Howe Hall, Room 2355, Ames, IA 50011-2271. Associate Fellow AIAA.

†Chief Research Engineer, 600 Pine Avenue. Member AIAA.

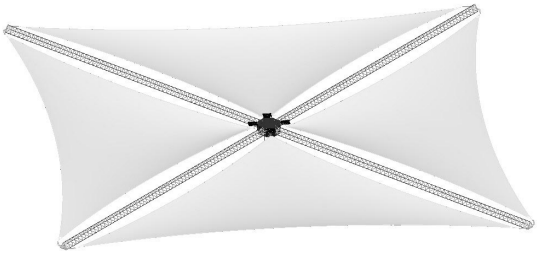

Fig. 1 A 20-m scalable solar sail by ATK Space Systems.

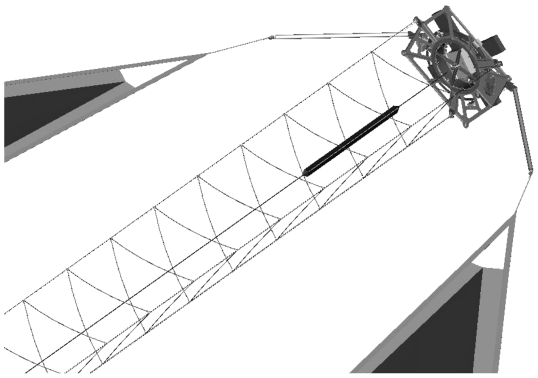

Fig. 2 ATK's solar-sail mast with a translating ballast mass (running along a lanyard tape), tip-mounted roll stabilizer bars attached to sail panels, and tip-mounted micro-PPT module.

friction, motor reliability, system redundancy, actuator lifetime, risk, and cost. Consequently, a recent solar-sail ACS tradeoff study resulted in a solar-sail ACS architecture using trim ballasts and roll stabilizer bars, integrated with a microthruster-based ACS, because of its overall simplicity, robust control authority, and low-risk advantages [6].

A solar-sail ACS architecture investigated in this paper consists of a propellantless primary ACS and a microthruster-based secondary ACS. The primary ACS employs trim ballasts running along mast lanyards for pitch/yaw control together with roll stabilizer bars (also called spreader bars) at the mast tips for quadrant tilt control (Fig. 2).

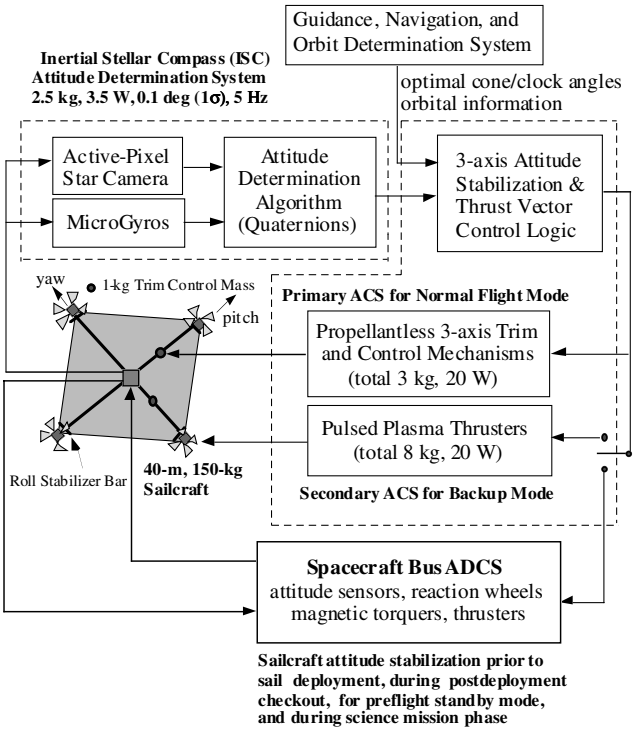

Fig. 3 An integrated ADCS architecture for solar sails.

The stability and robustness of such a propellantless primary ACS are further enhanced by a secondary ACS using tip-mounted, lightweight pulsed plasma thrusters (PPTs). Such a micro-PPT-based ACS can be employed for attitude recovery maneuvers from off-nominal conditions as well as for a spin-stabilized safe mode. It can also be employed as a backup to a conventional ACS (e.g., on a validation flight) before sail deployment and also during preflight sail checkout operation. The proposed solar-sail ACS will be applicable with minimal modifications to a wide range of future solar-sailing missions with varying requirements and mission complexity.

The attitude determination system (ADS) is a critical subsystem of the spacecraft attitude determination and control system (ADCS). An ADS of particular interest for solar-sail applications is the Inertial Stellar Compass (ISC) developed by Draper Laboratory for the New Millennium Program ST6 flight validation experiment [8]. The ISC is a miniature, low-power ADS developed for use with low-cost microsatellites. It is suitable for a wide range of future solar-sail missions because of its low-mass, low-power, and low-volume design and its self-initializing, autonomous operational capability. The ISC is composed of a wide field-of-view active-pixel star camera and microgyros, with associated data processing and power electronics. It has a total mass of 2.5 kg, a power requirement of 3.5 W, and an accuracy of 0.1 deg (1σ).

The proposed solar-sail ADCS architecture integrating various ADCS options, even including a conventional ADCS of sailcraft bus, is illustrated in Fig. 3. For most solar-sailing missions, a conventional spacecraft bus will be required but it may be jettisoned after sail deployment, depending on mission requirements. The recent advances in microsatellite bus technologies need to be exploited to develop such an integrated low-cost, low-risk, low-mass, and low-power ADCS of solar-sail spacecraft [8,9].

The remainder of this paper is outlined as follows: Sec. II discusses near-term solar-sail missions and the overall ACS requirements. Section III describes a solar-sail flight validation (SSFV) experiment proposed in a sun-synchronous orbit and its ACS requirements. In particular, a dawn–dusk sun-synchronous (DDSS) orbit is proposed for an SSFV experiment for demonstrating the simplicity, effectiveness, and robustness of the proposed solar-sail ACS. Various flight modes and ACS requirements for a spacecraft bus are also discussed in this section. Section IV describes the attitude equations of motion of a sailcraft in a DDSS orbit for attitude control design. Section V presents the primary ACS design employing trim ballasts and roll stabilizer bars. Section VI presents an overview of the state-of-the-art micro-PPT technology, lightweight PPT requirements for solar-sail applications, and a preliminary design of a micro-PPT-based secondary ACS for solar sails.

II. Near-Term Solar-Sail Missions and Attitude Control Requirements

A. Near-Term Solar-Sail Missions

Some potential near-term solar-sail missions envisioned by NASA are summarized in Table 1. The first three cases represent likely options for a near-Earth flight validation experiment. The first case is a low Earth orbit (LEO) sufficiently high to minimize the influence of atmospheric drag and atomic oxygen on solar sails. Such an orbit is attainable with several affordable dedicated launch options; however, the gravity-gradient disturbance torque can dominate the ACS design unless a particular low-Earth sun-synchronous (LSS) orbit and a proper sail orientation are selected as discussed later. The second is a geosynchronous transfer orbit

Table 1 Near-term solar-sail missions

Case	Mission description	Mission life	Size
LSS	1,600 km sun-synchronous	90 days	40 m
GTO	$2,000 \times 40,000$ km elliptic	90 days	40 m
GEO	36,000 km circular orbit	90 days	40 m
EMX	Earth Magnetotail Explorer	5 years	40 m
L1S	Lagrangian Point, 0.95 AU	5 years	80 m
SPI	Solar Polar Imager, 0.5 AU	5 years	160 m

(GTO), because this was the basis for a solar-sail study proposal to the New Millennium Program Space Technology 7. This orbit is attractive because the spacecraft would spend 80% of its time above 30,000 km, where the disturbance from gravity-gradient torques are negligible. The opportunity for a launch to GTO is restricted to secondary accommodation on a Delta II. The cost is very low, but the launch date and orbit are dictated by the primary payload mission and schedule. The third is a geosynchronous Earth orbit (GEO), which is included for comparison, although the cost of a launch to GEO is beyond the expected budget available for a sail validation flight. The three other flight mission cases are an Earth Magnetotail Explorer (EMX) mission in a $11R_\oplus \times 23R_\oplus$ Earth-centered elliptic orbit, an L_1 Sentinel (L1S), and the Solar Polar Imager (SPI), as discussed in [2].

For these near-term missions, solar sail sizes of 40, 80, and 160 m were chosen to allow the most straightforward scaling from the 80-m class hardware currently under development and test by ATK Space Systems [3,4]. The mass properties and the solar disturbance torques of such a scalable sailcraft are summarized in Table 2. An uncertainty of 0.25% of sail size is assumed for a preliminary estimation of the worst-case cm/cp offset. The pinwheel (windmill) disturbance torque about the roll axis is assumed to be about 50% of the pitch/yaw solar torque. Note that the solar disturbance torque is proportional to the cube of the sail size. Assumptions for masses of various components are based on hardware currently under development and in test. Variations are related to the scale of the sail and the timeline for launch. That is, the larger sails require larger structural geometry, but evolution of the engineering will allow some components to be more mass efficient. For example, the sail thickness will be reduced over time, as will the overall mass of integrated subsystems. Much uncertainty exists in the near-term capability of industry to build bus and payload hardware light enough to allow some future missions to be accomplished with reasonably sized sails. However, the masses and inertia of typical spacecraft bus and payload do not affect the overall sailcraft inertia, which is a primary input to the sail ACS sizing and design.

Table 2 Mass properties and solar disturbance torques of ATK's scalable sailcraft [3,4]

Sail size, m	40	80	160
Geometry			
Mast length, m	28	56	113
Mast diameter, m	0.4	0.4	0.6
Bending EI, N · m^2	82,441	82,441	438,847
Torsional GJ, N · m^2	197	197	453
Scallop factor, %	75	75	75
Sail area, m^2	1,200	4,800	19,200
Thrust (max), N	0.01	0.04	0.16
cm/cp offset,[a] m	0.1	0.2	0.4
Mass			
Sails, kg	6	19	67
Masts, kg	7	14	60
Tip mass (each), kg	1	2	2
Central assembly, kg	8	10	15
Sail ACS (primary), kg	3	5	7
Payload, kg	7	19	43
Bus (microsat), kg	50	75	100
Bus (standard), kg	150	200	250
Total (with microsat bus), kg	85	150	300
Total (with standard bus), kg	185	275	450
Acceleration (with micro bus), mm/s^2	0.11	0.26	0.53
Inertia			
I_x (roll), kg · m^2	4,340	40,262	642,876
I_y (pitch), kg · m^2	2,171	20,136	321,490
I_z (yaw), kg · m^2	2,171	20,136	321,490
Solar disturbance torque[b]			
Pitch/yaw, mN · m	1	8	64
Roll,[c] mN · m	0.5	4	32

[a]0.25% of the overall sail size is assumed for a nominally worst case.
[b]A nominally worst, maximum disturbance torque for untrimmed sailcraft.
[c]50% of the pitch/yaw solar torque is assumed for the windmill disturbance torque.

B. Attitude Control Requirements

For most near-term solar-sailing missions, the total sail flight system will probably consist of a solar sail and spacecraft bus. The spacecraft bus will provide all necessary mission supports before sail deployment and during preflight checkout operation.

The Earth-orbiting validation flights pose the most difficult challenges for sail ACS design. The environmental influences can complicate the measurement of solar thrust effects. Sail validation experiment planners are posed with a dilemma: Can an affordable launch and appropriate orbit be found that allows this promising interplanetary propulsion technology to first set sail beside the dangerous reefs (gravity-gradient torque, aerodrag, magnetic fields, thermal swings, plasma, orbital debris, and magnetospheric particles) of Earth's near-space environment? In general, low-thrust trajectories optimize with solutions where the thrust is throttleable (without shifting the nominal vector direction). Thus, a very maneuverable and redundant sailcraft is appropriate to provide robust thrust control authority for a broad class of sailing applications. This goal is pivotal in selecting the appropriate sail ACS concepts for near-term missions.

The attitude control requirements for a set of likely near-term solar-sailing missions have been quantitatively evaluated in [6]. A number of options for implementation of three-axis control has been traded using heuristic logic and first-order calculations. A preferable configuration for a robust ACS was determined based on the following requirements and criteria: 1) a demonstrated necessity to achieve agility (a neutrally stable configuration), 2) minimization of mass through functional overlap, 3) complete authority over maneuvering requirements of all missions, 4) large robustness margins for trimming potential offset asymmetries between the center of pressure and center of mass at the start of the mission, and 5) robust control over the sailcraft during deployment.

As illustrated in Fig. 3, the baseline solar-sail ACS architecture chosen for near-term solar-sailing missions consists of 1) the propellantless primary ACS employing trim ballasts for pitch/yaw control and roll stabilizer bars, 2) the secondary ACS using tip-mounted, lightweight pulsed plasma thrusters, and 3) the spacecraft bus ACS.

The trim actuator positions for balancing at the nominal orientation may not provide precise trim for substantially different sailcraft orientations. Trim balance can be enhanced by integrating the mechanical balance system with thruster firing. For example, an excessive firing rate of one thruster will command the balance system to adjust on the related control axis. The autotrimming control system will result in low-frequency, two-sided limit cycle thruster firings within the attitude error deadband required by navigation and payload pointing requirements. The proposed sailcraft ACS architecture possesses large stability margins, multiple redundancies, and the agility to enable the thrust vector and thrust magnitude to be adjusted independently to optimize low-thrust trajectories. It also provides a full three-axis, robust control authority for any sail orientation including an edge-on flight orientation toward the sun. The proposed sail flight control system architecture will be applicable with minimal modifications to a wide range of future solar-sail flight missions with varying requirements and mission complexity.

III. Solar-Sail Flight Validation Mission

A. Orbit Selection Issue for an SSFV Mission

The New Millennium Program (NMP) Space Technology (ST) program function is to flight-validate promising spacecraft technologies. The benefits of propellantless propulsion for enabling a broad spectrum of future science missions at low cost have long been recognized. The NMP has solicited and/or funded Phase A solar-sail studies on Space Technology 5, 6, 7, and 8. A key impediment to selection for flight of solar-sail system technology has been the cost of a dedicated launch to a higher orbit. The previous sail system proposal to the NMP ST7 advocated to fly a small sailcraft as a secondary on the Evolved Secondary Payload Adaptor (ESPA) ring aboard a Delta II launch vehicle to a GTO or a supersynchronous

transfer orbit (SSTO). The projected cost of this form of space access is very low. However, secondary opportunities on larger launchers have hidden cost, as often payloads are bumped several times before funding, the right launch opportunity, and the readiness of the payload come together.

For the next NMP ST9 there is anticipated a slightly larger budget and the desire for a dedicated launcher persists. Pegasus, Minotaur, PeaceKeeper, and Falcon are some of the lower-cost launch vehicle options that can reach an appreciable altitude. Pegasus and Minotaur have very similar capabilities: 150 kg to 1000 km ($i = 99.5$ deg). Pegasus XL can launch 273 kg to 1250-km circular orbit. PeaceKeeper and Falcon are new launch vehicles that will be flying before the year anticipated for a sailcraft validation flight. These vehicles will allow a larger sailcraft volume and can place more mass into a high LEO. For example, the Falcon vehicle can place over 400 kg in a 1000-km sun-synchronous orbit. PeaceKeeper will lift even more, but the added cost would consume a large fraction of the available mission budget, as would Pegasus or Minotaur, which are only viable if the sail and spacecraft mass are quite minimal. Comparisons of the available payload accommodation and rough costs can be found in [6].

B. SSFV Mission in a Dawn–Dusk Sun-Synchronous Orbit

Given that one or two new launch systems, such as PeaceKeeper and Falcon, may be available to cost-effectively place a sailcraft into a high LEO flight validation orbit, a particular DDSS orbit is chosen to examine the ramifications on sail ACS architecture selection and design.

1. *Dawn–Dusk Sun-Synchronous Orbit*

A circular sun-synchronous orbit is characterized by its nodal regression rate $\dot{\Omega}$ as follows:

$$\dot{\Omega} \approx -\frac{3J_2R_\oplus^2}{2a^2} n \cos i \tag{1}$$

where $R_\oplus$ is the Earth's radius, $J_2 = 0.001082$ is the Earth's oblateness, $n = \sqrt{\mu/a^3}$, μ is the Earth's gravitational parameter, $a = R_\oplus + h$, h is the orbital altitude, and i is the inclination [10,11].

The Earth revolves around the sun in a nearly circular orbit ($e = 0.016726$) with a period of 365.24 solar days. The Earth also rotates about its own axis with a period of one siderial day (23 h 56 min 4.09 s). The sun-synchronous orbit has a nodal regression rate $\dot{\Omega}$ equal to the Earth's mean rate of revolution around the sun (i.e., 360 deg in 365.24 solar days or 0.985 deg/day). This regression must be in the direction of the Earth's rotation because the Earth rotates about its axis in the same direction that it revolves around the sun. Therefore, a sun-synchronous satellite must have a retrograde orbit so its nodal regression can be prograded. Also, the satellite must have a combination of altitude and inclination that produces 0.985 deg/day regression. The sun-synchronous orbits maintain their initial orientation relative to the sun. Such retrograde orbits lie between inclination angles of 95.7 and 180 deg at altitudes up to 5970 km. Sun-synchronous orbits below 1400 km can experience some shadowing and the orbital debris density remains significant from 1400 to 1550 km. As these environments pose some hazard to a sailcraft, a preferable orbit may be in the range of 1600 km. The Falcon launch system can place a 300-kg spacecraft at this altitude in the proper synchronous (102.5 deg) orbit. It is desirable to avoid shadowing, as the penumbra transits will cause rapid thermal shocks that will dynamically excite the structure, stress the sail, and swiftly exercise the negator mechanisms used to maintain constant sail tension. Eclipse will also cause large charging swings, and the effects on a large sail may be detrimental. These issues should be explored further, but at present the aggregate benefits of a 1600-km orbit with $i = 102.5$ deg, $n = 8.86\text{e-}4$ rad/s, and an orbital period of 118.2 min are enticing.

If the launch is scheduled to place the sailcraft in a dawn–dusk orientation the line of nodes will be (always) perpendicular to the sun line and on two occasions per year the orbit will be normal to the sun. For a short-duration sail-validation experiment, the opportunity exists to conduct operations with the orbit plane nearly normal to the sun. There are two windows per year, beginning near the vernal equinox (for a dusk launch) or the autumn equinox (for a dawn launch) where the so-called sun angle β will remain within 10 deg for nearly six months.

In contrast to the GTO, a DDSS orbit would mean the following:

1) The sailcraft would not need a propulsion stage to lift the perigee to 2000 km.

2) The nominal orientation of the sail could be kept nearly in plane with the orbit plane, thus minimizing the gravity-gradient disturbance torque.

3) The sailcraft would not pass through the Van Allen belts. The environmental effects of high radiation on the sails are not yet quantified. Additional shielding mass will not be required on all electronics.

4) The thermal environment for the bus would have reduced variations.

5) Operational ranging and communication may be simplified.

In summary, the DDSS orbit will require a simpler spacecraft design than a GTO mission for ACS, thermal control, power, communications, and propulsion. The effect on mission cost through reduced spacecraft systems engineering, production, and testing may be quite significant. Reductions in ACS elements, thermal control apparatus, battery size, solar arrays, antenna size, and perhaps lower radiation shielding will result in an overall lower sailcraft mass. This will improve sailing performance and may allow an extended mission where the orbit is significantly modified or perhaps even Earth escape could be achieved, freeing the sailcraft for an interplanetary journey.

2. *Zero-Thrust Mode (Sail Deployment Mode)*

After orbit insertion into the DDSS orbit, the first major task is completion of a successful solar-sail deployment. Large sails take a considerable time to deploy, and if management of unfolding sails becomes unsynchronized, solar pressure will place a large torque on the sailcraft and would quickly accelerate any free section. To minimize the consequences of such events it would be prudent to orient edge-on to the sun initially, as illustrated in Fig. 4. If the sailcraft were continuously aligned with the nadir line as illustrated in Fig. 4, the sailcraft would be gravity-gradient stabilized in pitch with negligible gravity-gradient torque in roll. In fact, the roll, pitch, and yaw axes of the sailcraft in this zero-thrust mode are to be aligned with the local-vertical and local-horizontal (LVLH) reference frame. Consequently, a conventional bus ACS can be employed for this

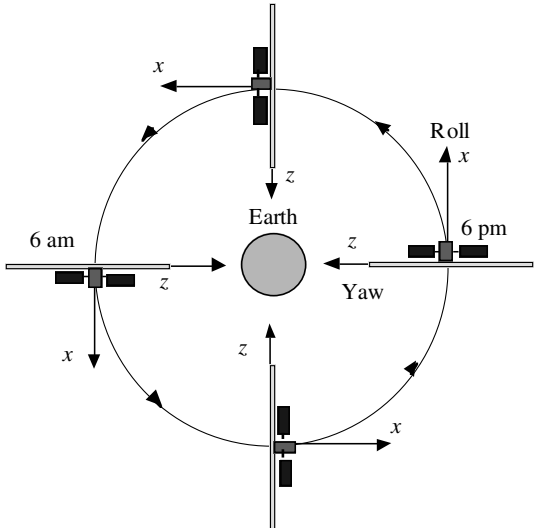

Fig. 4 Gravity-gradient stable sail flight orientation of the zero-thrust mode (sail deployment mode) for sail deployment and initial checkout. The sun vector is perpendicular to the orbit plane with an offset sun angle β.

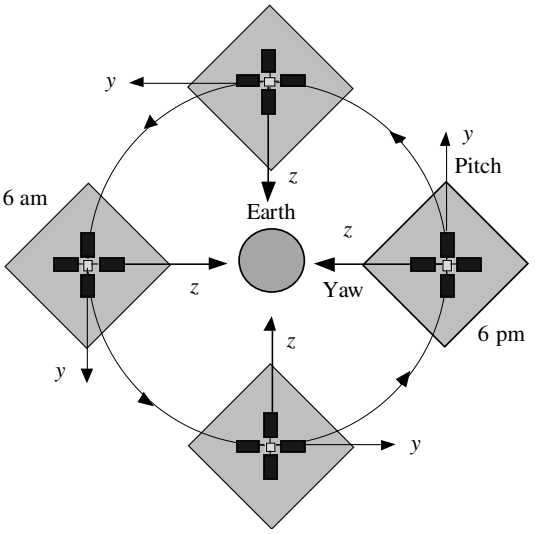

Fig. 5 Sail flight orientation for the full-thrust standby mode (sun-pointing mode); no significant orbital effects of the solar thrust.

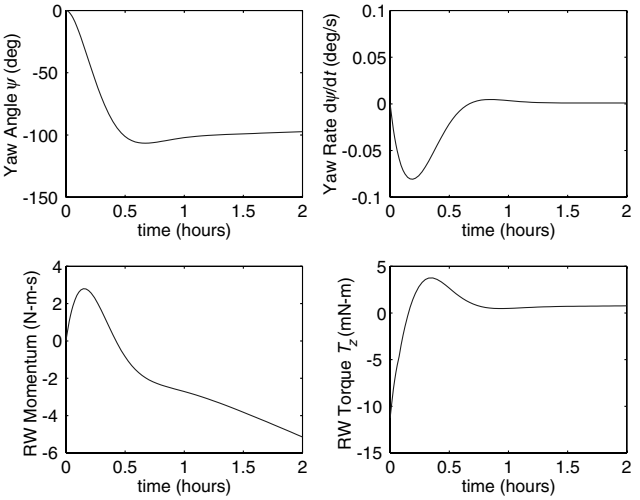

Fig. 7 A −90 deg yaw maneuver of an untrimmed 40-m sailcraft (with cm/cp offset of 0.1 m) using a reaction wheel for transition to the standby full-thrust mode.

fully deployed sailcraft only during the zero-thrust mode operation without the presence of significant solar pressure disturbance torques. During this zero-thrust "safe" mode operation, various initial testing and checkout of the fully deployed sailcraft can be safely conducted. A proper orientation/articulation of the solar arrays of sail carrier spacecraft would be required for long-duration zero-thrust mode operation.

3. Yaw Reorientation Mode

After successful sail deployment and completion of checkout activities in the zero-thrust mode, a −90 deg yaw maneuver will then be needed to achieve the proper sail orientation of the full-thrust standby mode illustrated in Fig. 5. The orbit would be nearly normal to the sun line if the launch were timed for the minimal sun angle β, which varies with the season.

The conventional bus ACS (or the tip-mounted microthruster system) is best suited to perform this reorientation about the yaw axis, as the ballast masses have negligible control authority when the sail is oriented near edge-on to the sun. As indicated in Figs. 6 and 7, a transition to the propellantless sail ACS will be required, immediately after achieving the desired yaw orientation to avoid excessive propellant usage or excessive wheel momentum growth for counteracting the solar disturbance torque. For simulations in Fig. 6, a 0.1-N thruster with a 0.5-m moment arm was assumed. As can be noticed in Fig. 7, a small reaction wheel cannot be employed for such a maneuver because a typical 2-kg wheel with a peak torque of 0.01 N · m has less than 2 N · m · s momentum storage capability. Although small magnetic torquers can be employed for momentum dumping as discussed in [9], such a combination of reaction wheels and magnetic torquers is not examined in this paper because most solar sails will be primarily used for interplanetary missions. While the sailcraft is held on-sun by a thruster-based ACS of spacecraft bus, the trim ballast system and roll stabilizer bars would be activated to trim the transverse solar torque and also null any pinwheel motion. For Figs. 6 and 7, a dynamical model of sailcraft in the DDSS orbit was used, which will be discussed in Sec. IV.

4. Full-Thrust Standby Mode (Sun-Pointing Mode)

After successful sail deployment, further key validations of sail technology can begin: the demonstration of effective propulsion and robust steering control of the solar thrust vector. At a minimum, it is proposed that attitude maneuvers and orbit-changing propulsion be validated. The sun line would be nearly normal to the orbital plane if the launch were timed to the seasonal variations in sun angle β. Although the sailcraft is at full thrust, the orbital motion is not much affected by the solar pressure force when it is nearly perpendicular to the orbital plane, as can be seen in Fig. 8. Note that the nodal regression rate of 1 deg/day is still maintained.

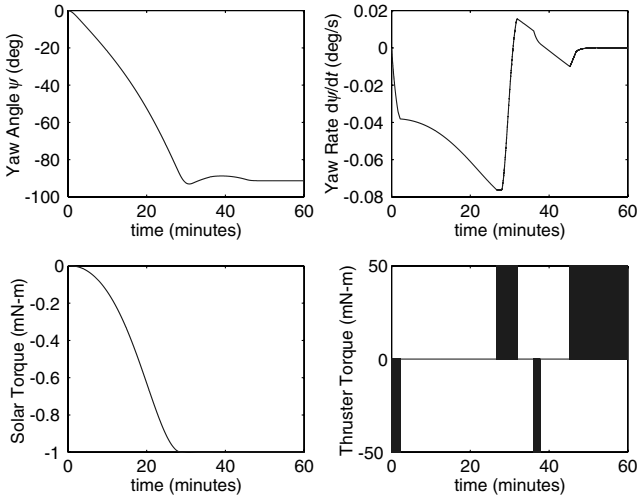

Fig. 6 A −90 deg yaw maneuver of an untrimmed 40-m sailcraft (with cm/cp offset of 0.1 m) using reaction jets for transition to the standby full-thrust mode.

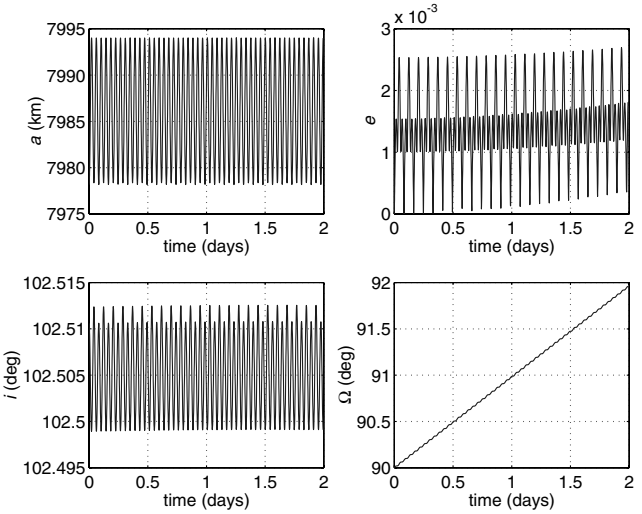

Fig. 8 Dawn–dusk sun-synchronous orbit simulation of the full-thrust standby mode.

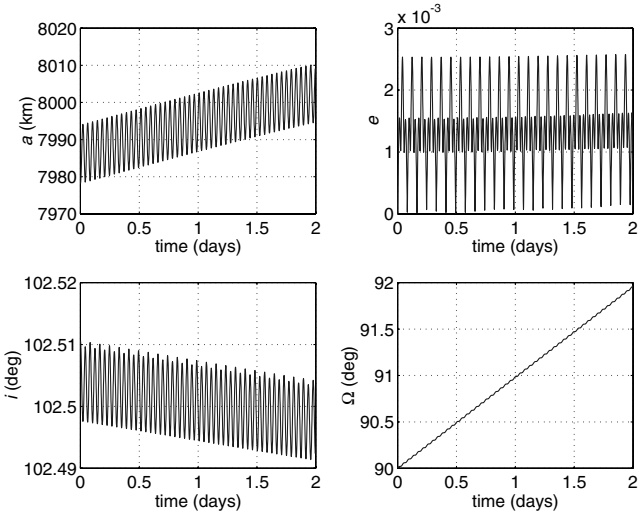

Fig. 9 Dawn–dusk sun-synchronous orbit simulation of the TVC mode: an 8 km/day orbit raise.

5. Thrust Vector Control Mode

A constant yaw angle of −55 deg (equivalently, a 35-deg tilt angle of the roll axis relative to the sun line) will add energy to the orbit. Therefore, a reorientation maneuver back to a yaw angle of −55 deg will be needed to continuously increase the orbital energy. It may be possible to alternate the yaw angle to maintain the orbit as operational confidence is developed. Over time the ability to orient for viewing from the ground may be tested. The validation may conclude with an intentional deorbit, unless the thrust to mass ratio allows an Earth escape. Simulation results of the thrust vector control (TVC) mode indicate that approximately 8 km/day orbit-raising will be possible as shown in Fig. 9.

IV. Attitude Dynamics of a Sailcraft with Translating Control Masses

The problem of a spacecraft with internal moving mass was first investigated in the early 1960s. For spacecraft dynamical problems with internal moving mass, one may choose the composite center of mass of the total system as a reference point for the equations of motion. This formulation leads to a time-varying inertia matrix, because the reference point moves as the internal mass moves relative to the main body. On the other hand, one may choose the center of mass of the main body as the reference point, which leads to a constant inertia matrix of the main body relative to the reference point, but results in complex equations of motion. Because of the convenience of dealing with a constant inertia matrix of the main body, we employ the second approach of choosing the center of mass of the main body as the reference point for a sailcraft with moving trim ballasts.

A. Formulation of a Dynamical Model

Consider a sailcraft in an Earth-centered orbit as illustrated in Fig. 10. The sailcraft has the body-fixed principal axes as indicated in this figure. The roll axis is perpendicular to the sail plane and it often nominally points toward the sun (but not necessarily). The pitch and yaw axes are the transverse axes along the masts. The dynamical model consists of a rigid sailcraft of mass M and two trim ballasts of each mass of m, as shown in Fig. 10. The origin of the body-fixed reference frame with a set of basis vectors $\{\boldsymbol{i}, \boldsymbol{j}, \boldsymbol{k}\}$ is located at point O, which is assumed to be the center of mass of a sailcraft of mass M excluding the ballast masses. It is also assumed that ballasts are running along mast lanyards (i.e., along the pitch and yaw axes).

For a spacecraft with translating control masses, as discussed in [10,11], one may choose the angular momentum equation as

$$\dot{\boldsymbol{h}}_o + (M + 2m)\boldsymbol{r}_c \times \boldsymbol{a}_o = \boldsymbol{G} \tag{2}$$

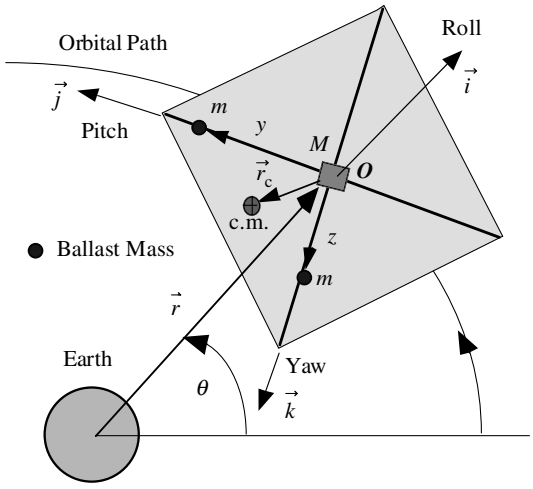

Fig. 10 A solar-sail spacecraft with translating trim ballasts in an Earth-centered orbit.

where $\boldsymbol{h}_o$ is the relative angular momentum of the total system about point O, $(M + 2m)$ is the total mass, $\boldsymbol{a}_o$ is the inertial acceleration of the point O, $\boldsymbol{G}$ is the gravity-gradient torque vector about the point O, and $\boldsymbol{r}_c$ is the position vector of the composite center of mass from the reference point O given by

$$\boldsymbol{r}_c = \frac{m}{M + 2m}(y\boldsymbol{j} + z\boldsymbol{k}) \tag{3}$$

The relative angular momentum of the total system about point O is given by

$$\boldsymbol{h}_o = \hat{I} \cdot \boldsymbol{\omega} + my\boldsymbol{j} \times \frac{\mathrm{d}}{\mathrm{d}t}(y\boldsymbol{j}) + mz\boldsymbol{k} \times \frac{\mathrm{d}}{\mathrm{d}t}(z\boldsymbol{k}) \tag{4}$$

where $\hat{I}$ is inertia dyadic of the total system when the ballast is not moving and $\boldsymbol{\omega}$ is the angular velocity vector of the main body (i.e., the sail platform) expressed as

$$\boldsymbol{\omega} = \omega_x\boldsymbol{i} + \omega_y\boldsymbol{j} + \omega_z\boldsymbol{k} \tag{5}$$

The inertia dyadic of the total system, including the ballast mass, about the reference point O is given by [10]

$$\hat{I} = \begin{bmatrix} \boldsymbol{i} & \boldsymbol{j} & \boldsymbol{k} \end{bmatrix} \begin{bmatrix} \tilde{I}_x & 0 & 0 \\ 0 & \tilde{I}_y & 0 \\ 0 & 0 & \tilde{I}_z \end{bmatrix} \begin{bmatrix} \boldsymbol{i} \\ \boldsymbol{j} \\ \boldsymbol{k} \end{bmatrix}$$

where $\tilde{I}_x = I_x + m(y^2 + z^2)$, $\tilde{I}_y = I_y + mz^2$, $\tilde{I}_z = I_z + my^2$, and (I_x, I_y, I_z) are the principal moments of inertia of the sailcraft, not including the ballast mass m.

The inertial acceleration of the reference point O is related to the inertial acceleration of the composite center of mass as

$$\boldsymbol{a}_o = \boldsymbol{a}_c - \ddot{\boldsymbol{r}}_c = \frac{\boldsymbol{F}}{M + 2m} - \frac{m}{M + 2m}\frac{\mathrm{d}^2}{\mathrm{d}t^2}(y\boldsymbol{j} + z\boldsymbol{k}) \tag{6}$$

where $\boldsymbol{F}$ is the solar-radiation-pressure force vector acting on the sailcraft.

The attitude equation of motion, Eq. (2), can then be rewritten as

$$\frac{\mathrm{d}}{\mathrm{d}t}\left(\hat{I} \cdot \boldsymbol{\omega} + my\boldsymbol{j} \times \frac{\mathrm{d}}{\mathrm{d}t}(y\boldsymbol{j}) + mz\boldsymbol{k} \times \frac{\mathrm{d}}{\mathrm{d}t}(z\boldsymbol{k})\right) + \frac{m}{M + 2m}(y\boldsymbol{j} + z\boldsymbol{k}) \times \left[\boldsymbol{F} - m\frac{\mathrm{d}^2}{\mathrm{d}t^2}(y\boldsymbol{j} + z\boldsymbol{k})\right] = \boldsymbol{G} \tag{7}$$

Ignoring the various nonlinear terms associated with $\dot{y}$, $\dot{z}$, etc., and by expressing $\boldsymbol{F}$ and $\boldsymbol{G}$ as

$$\boldsymbol{F} = F_x\boldsymbol{i} + F_y\boldsymbol{j} + F_z\boldsymbol{k} \qquad \boldsymbol{G} = G_x\boldsymbol{i} + G_y\boldsymbol{j} + G_z\boldsymbol{k}$$

we obtain the attitude equations of motion as

$$J_x\dot{\omega}_x = (J_y - J_z)\omega_y\omega_z - \frac{m_r}{M+m}(yF_z - zF_y) + G_x \tag{8}$$

$$J_y\dot{\omega}_y = (J_z - J_x)\omega_z\omega_x - \frac{m_r}{M+m}zF_x + G_y \tag{9}$$

$$J_z\dot{\omega}_z = (J_x - J_y)\omega_x\omega_y + \frac{m_r}{M+m}yF_x + G_z \tag{10}$$

where m_r is the so-called reduced mass defined as

$$m_r = \frac{m(M+m)}{M+2m} \tag{11}$$

and

$$J_x = I_x + m_r(y^2 + z^2) \qquad J_y = I_y + m_r z^2 \qquad J_z = I_z + m_r y^2$$

For solar-sail applications, we have $m_r \approx m$ because $M \gg m$.

B. Sailcraft Attitude Dynamics in a DDSS Orbit

For the description of angular orientations of sailcraft in an Earth-centered circular orbit, the LVLH reference frame is considered here. This LVLH frame with its origin at the center of mass of an orbiting sailcraft has a set of unit vectors $\{\boldsymbol{a}_1, \boldsymbol{a}_2, \boldsymbol{a}_3\}$ with $\boldsymbol{a}_3$ locally vertical toward the Earth, $\boldsymbol{a}_1$ along the locally horizontal (transverse) direction, and $\boldsymbol{a}_2$ perpendicular to the orbit plane. The body-fixed reference frame B has a set of basis vectors $\{\boldsymbol{i}, \boldsymbol{j}, \boldsymbol{k}\}$. The relative orientation of the sailcraft with respect to the LVLH frame is described by three Euler angles (ϕ, θ, ψ) of the rotational sequence of $\mathbf{C}_1(\phi) \leftarrow \mathbf{C}_2(\theta) \leftarrow \mathbf{C}_3(\psi)$ from the LVLH to B.

The angular velocity components of the sailcraft are then given by [10]

$$\begin{bmatrix}\omega_x\\ \omega_y\\ \omega_z\end{bmatrix} = \begin{bmatrix}1 & 0 & -\sin\theta\\ 0 & \cos\phi & \sin\phi\cos\theta\\ 0 & -\sin\phi & \cos\phi\cos\theta\end{bmatrix}\begin{bmatrix}\dot{\phi}\\ \dot{\theta}\\ \dot{\psi}\end{bmatrix} - n\begin{bmatrix}\cos\theta\sin\psi\\ \sin\phi\sin\theta\sin\psi + \cos\phi\cos\psi\\ \cos\phi\sin\theta\sin\psi - \sin\phi\cos\psi\end{bmatrix} \tag{12}$$

where $n = \sqrt{\mu/a^3}$ is the orbital rate and (ϕ, θ, ψ) are called the roll, pitch, and yaw angles of a spacecraft relative to the LVLH orientation. The kinematic differential equations can then be found as

$$\begin{bmatrix}\dot{\phi}\\ \dot{\theta}\\ \dot{\psi}\end{bmatrix} = \frac{1}{\cos\theta}\begin{bmatrix}\cos\theta & \sin\phi\sin\theta & \cos\phi\sin\theta\\ 0 & \cos\phi\cos\theta & -\sin\phi\cos\theta\\ 0 & \sin\phi & \cos\phi\end{bmatrix}\begin{bmatrix}\omega_x\\ \omega_y\\ \omega_z\end{bmatrix} + \frac{n}{\cos\theta}\begin{bmatrix}\sin\psi\\ \cos\phi\cos\psi\\ \sin\theta\sin\psi\end{bmatrix} \tag{13}$$

The gravity-gradient torque components are given by

$$G_x = -3n^2(J_y - J_z)R_yR_z \tag{14a}$$

$$G_y = -3n^2(J_z - J_x)R_zR_x \tag{14b}$$

$$G_z = -3n^2(J_x - J_y)R_xR_y \tag{14c}$$

where $R_x = -\sin\theta$, $R_y = \sin\phi\cos\theta$, and $R_z = \cos\phi\cos\theta$. For small roll/pitch angles, the gravity-gradient disturbance torques become

$$G_x = -3n^2(J_y - J_z)\phi \tag{15a}$$

$$G_y = -3n^2(J_x - J_z)\theta \tag{15b}$$

$$G_z = 0 \tag{15c}$$

Note that there is no gravity-gradient torque about the yaw axis and that the gravity-gradient torque about the roll axis becomes zero when $J_y = J_z$.

Finally, we obtain the attitude equations of motion as follows:

$$J_x\dot{\omega}_x = (J_y - J_z)\omega_y\omega_z - 3n^2(J_y - J_z)\phi + 0.5\epsilon F + T_x \tag{16a}$$

$$J_y\dot{\omega}_y = (J_z - J_x)\omega_z\omega_x - 3n^2(J_x - J_z)\theta + \frac{m_r}{M+m}zF + \epsilon F + T_y \tag{16b}$$

$$J_z\dot{\omega}_z = (J_x - J_y)\omega_x\omega_y - \frac{m_r}{M+m}yF + \epsilon F + T_z \tag{16c}$$

where (T_x, T_y, T_z) are the control torques generated by reaction wheels, thrusters, or roll stabilizer bars. The solar-radiation-pressure force is assumed here as: $\boldsymbol{F} = F_x\boldsymbol{i} = -F\boldsymbol{i}$ and $F = F_s\cos^2\alpha$, where $F_s \equiv \eta PA$ is the maximum sail thrust, η is the overall sail thrust coefficient ($\eta_{\max} = 2$), $P = 4.563 \times 10^{-6}$ N/m^2, A is the total sail area, and α is the sun angle between the sun line and the roll axis. It is also assumed that the cm/cp distance has an uncertainty of ϵ. The roll-axis solar disturbance torque is assumed as 50% of the pitch/yaw solar disturbance torque ϵF.

For large-angle reorientations about the yaw axis (during a transition from the zero-thrust mode to the full-thrust mode), but with small roll and pitch angles, we have

$$\omega_x \approx \dot{\phi} - n\sin\psi \tag{17a}$$

$$\omega_y \approx \dot{\theta} - n\cos\psi \tag{17b}$$

$$\omega_z \approx \dot{\psi} - n(\theta\sin\psi - \phi\cos\psi) \tag{17c}$$

The final set of attitude equations of motion for the design and simulation of the various sail flight modes in a DDSS orbit, as illustrated in Figs. 4 and 5, can then be obtained as

$$J_x\ddot{\phi} + n^2(J_y - J_z)(3 + \cos^2\psi)\phi - n^2(J_y - J_z)(\cos\psi\sin\psi)\theta - n(J_x - J_y + J_z)(\cos\psi)\dot{\psi} = 0.5\epsilon F + T_x \tag{18}$$

$$J_y\ddot{\theta} + n^2(J_x - J_z)(3 + \sin^2\psi)\theta - n^2(J_x - J_z)(\cos\psi\sin\psi)\phi - n(J_x - J_y - J_z)(\sin\psi)\dot{\psi} = \frac{Fm_r}{M+m}z + \epsilon F + T_y \tag{19}$$

$$J_z\ddot{\psi} + n^2(J_y - J_x)\sin\psi\cos\psi + n(J_x - J_y + J_z)(\cos\psi)\dot{\phi} + n(J_x - J_y - J_z)(\sin\psi)\dot{\theta} = -\frac{Fm_r}{M+m}y + \epsilon F + T_z \tag{20}$$

where $F = F_s\cos^2\alpha$. It is further assumed that the sun angle $\beta \approx 0$ and $\alpha = \pi/2 + \psi$. Note that the zero-thrust mode has a zero-yaw angle and that the full-thrust mode has a yaw angle of -90 deg.

For a special case of standard spacecraft with small roll/pitch/yaw angles relative to the LVLH reference frame, we obtain the well-known attitude equations of motion of the following form [10]:

$$J_x\ddot{\phi} + 4n^2(J_y - J_z)\phi - n(J_x - J_y + J_z)\dot{\psi} = T_x \tag{21}$$

$$J_y\ddot{\theta} + 3n^2(J_x - J_z)\theta = T_y \tag{22}$$

$$J_z\ddot{\psi} + n^2(J_y - J_x)\psi + n(J_x - J_y + J_z)\dot{\phi} = T_z \tag{23}$$

V. Preliminary Design of the Propellantless Primary ACS

Ignoring the coupling terms in Eqs. (18–20), one can design sail attitude control logic for each axis as described in this section. A 40-m, 150-kg sailcraft is assumed here.

A. Yaw-Axis Control Design

A yaw-axis control design model, as illustrated in Fig. 11, is assumed as

$$J_z\ddot{\psi} + \frac{1}{2}n^2(J_y - J_x)\sin 2\psi = -\frac{F_s\cos^2\alpha m_r}{M+m}y + \epsilon F_s\cos^2\alpha \tag{24}$$

where $J_x = I_x + m_r(y^2 + z^2), J_y = I_y + m_r z^2, J_z = I_z + m_r y^2, \psi$ is the yaw angle defined as $\psi = -\pi/2 + \alpha$, and m_r is the reduced mass defined as $m_r = m(M+m)/(M+2m) \approx m$. The steady-state trim position of the ballast for countering the effect of the cm/cp offset ϵ can be estimated as

$$y_{ss} = \frac{M+m}{m_r}\epsilon \approx \frac{M}{m}\epsilon \tag{25}$$

The actuator dynamics of the translating ballast mass is assumed as

$$T\dot{y} + y = y_c; \qquad |y_c(t)| \le y_{\max} \tag{26}$$

where T is the actuator time constant, y is the actual position, and y_c is the commanded position (the control input) with a maximum value of $y_{\max}$. The maximum speed $\dot{y}_{\max}$ can be estimated as

$$\dot{y}_{\max} = \frac{y_{\max}}{T} \tag{27}$$

As an example, we have $y_{ss} = \pm 14.9$ m and $\dot{y}_{\max} = \pm 0.05$ m/s for a 40-m, 150-kg sailcraft with $M = 148$ kg, $m = 1$ kg, $\epsilon = \pm 0.1$ m, $y_{\max} = \pm 28$ m, and $T = 560$ s.

Consider a feedback control logic of the form [12,13]

$$y_c = \underset{y_{\max}}{\text{sat}}\left\{K_p \underset{L}{\text{sat}}(e) + K_d\dot{\psi}\right\} \tag{28}$$

where $e = \psi - \psi_c$, and K_p and K_d are, respectively, the attitude and attitude rate gains to be properly determined. The saturation function is defined as

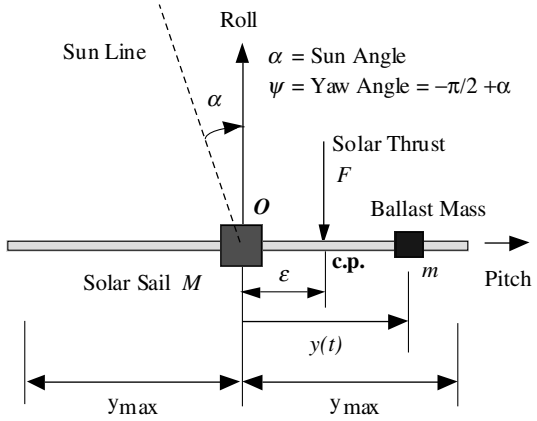

Fig. 11 A yaw-axis dynamic model of sailcraft with a translating ballast mass.

$$\underset{L}{\text{sat}}(e) = \begin{cases} L & \text{if } e \ge L \\ e & \text{if } |e| < L \\ -L & \text{if } e \le -L \end{cases} \tag{29}$$

and it can also be represented as

$$\underset{L}{\text{sat}}(e) = \text{sgn}(e)\min\{|e|, L\} \tag{30}$$

Because of the presence of a limiter in the attitude-error feedback loop, the attitude rate becomes constrained as

$$-\dot{\psi}_{\max} \le \dot{\psi} \le \dot{\psi}_{\max} \tag{31}$$

where $\dot{\psi}_{\max} = LK_p/K_d$.

Furthermore, if the maximum slew rate is specified as $|\dot{\psi}|_{\max}$, then the limiter in the attitude-error feedback loop can be selected simply as

$$L = \frac{K_d}{K_p}\dot{\psi}_{\max} \tag{32}$$

However, as the attitude-error signal gets larger and also as the slew rate limit becomes larger for rapid maneuvers, the overall response becomes sluggish with increased transient overshoot because of the actuator saturation. To achieve rapid transient settlings even for large commanded attitude angles, the slew rate limit needs to be adjusted as follows:

$$\dot{\psi}_{\max} = \min\{\sqrt{2a|e|}, \omega_{\max}\} \tag{33}$$

where $\omega_{\max}$ is the specified maximum slew rate, and a is the maximum angular acceleration described by

$$a = \frac{F_s m_r y_{\max}}{J_z M + m} \tag{34}$$

A smaller value than the nominal a may be used to accommodate various uncertainties in the spacecraft inertia and actuator dynamics. Such a variable limiter in the attitude-error feedback loop has the self-adjusting saturation limit as

$$L = \frac{K_d}{K_p}\min\{\sqrt{2a|e|}, \omega_{\max}\} \tag{35}$$

If an integral control is necessary to eliminate a steady-state pointing error due to the constant external disturbance caused by a cm/cp offset, the feedback control logic (28) can be further modified into the nonlinear proportional-integral-derivative (PID) control logic of the form [12,13]

$$y_c = \underset{y_{\max}}{\text{sat}}\left\{K_p \underset{L}{\text{sat}}\left[(\psi - \psi_c) + \frac{1}{\tau}\int(\psi - \psi_c)\right] + K_d\dot{\psi}\right\} \tag{36}$$

where τ is the time constant of integral control and L is given by Eq. (36).

For a nonlinear PID control logic of the form (36), the so-called integrator antiwindup or integrator synchronization is necessary to avoid the phenomenon known as integrator windup, inherent to all PID-type controllers with actuator saturation. Such integrator windup results in substantial transient overshoot and control effort. If the controller is implemented on a digital computer, integrator antiwindup can be simply achieved by turning off the integral action as soon as the actuator or any other limiter in the control loop saturates.

B. Pitch-Axis Control Design

Similar to the yaw-axis control design, the pitch-axis control logic for a translating control mass along the z axis is assumed as

$$z_c = -\underset{z_{\max}}{\text{sat}}\left\{K_p \underset{L}{\text{sat}}\left[(\theta-\theta_c)+\frac{1}{\tau}\int(\theta-\theta_c)\right]+K_d\dot{\theta}\right\} \tag{37}$$

where z_c is the commanded position of the control mass.

C. Roll-Axis Control Design

The roll-axis control logic of the roll stabilizer bar (RSB) is also assumed as

$$T_x = -\underset{T_{\max}}{\text{sat}}\left\{K_p \underset{L}{\text{sat}}\left[(\phi-\phi_c)+\frac{1}{\tau}\int(\phi-\phi_c)\right]+K_d\dot{\phi}\right\} \tag{38}$$

where T_x is the roll control torque command with a saturation limit of $T_{\max}$.

The roll control torque T_x (in units of $\mathrm{N}\cdot\mathrm{m}$) is related to the tilt angle Θ of the RSB of an assumed length of 1 m for a baseline 40-m sailcraft, as follows:

$$T_x = (0.5/20)(13.3)F_s \sin\Theta \tag{39}$$

where it is assumed that all four RSBs are rotated simultaneously. Consequently, we have $T_{\max}$ of ± 2.3 $\mathrm{mN}\cdot\mathrm{m}$ for a maximum tilt angle of ± 45 deg.

The RSB actuator dynamics is also assumed as

$$T\dot{\Theta}+\Theta=\Theta_c; \qquad |\Theta_c(t)| \le \Theta_{\max} \tag{40}$$

where T is the actuator time constant, Θ is the actual tilt angle, and Θ_c is the commanded tilt angle (the control input) with a maximum value of $\Theta_{\max}$. The commanded tilt angle of the RSB is then given by

$$\Theta_c = \arcsin\left\{\frac{20T_x}{(0.5)(13.3)F_s}\right\} \tag{41}$$

D. Three-Axis Coupled Dynamic Simulation

The effectiveness of the proposed sail attitude control logic was validated using three-axis coupled dynamic simulations. Simulation results of the TVC mode with $\psi_c = -55$ deg are shown in Fig. 12. A 35-deg yaw maneuver, while maintaining small roll/pitch attitude errors, is performed within the saturation limits of propellantless control actuators. This case confirms the feasibility of demonstrating an orbit raising maneuver in a 1600-km DDSS orbit by employing the proposed propellantless primary ACS. More detailed discussions of the proposed propellantless ACS can be found in [14–17].

VI. Micro-PPT-Based Secondary ACS

A secondary ACS, using tip-mounted, lightweight pulsed plasma thrusters (PPT), is described in this section. Such a microthruster-based ACS provides reliable capability for recovery of attitude given any off-nominal conditions, including tumbling, that cannot be handled by either the propellantless primary ACS or by conventional ACS within the sail spacecraft bus. Micro-PPT-based ACS is also useful for three-axis stabilization of the sailcraft after release from the launch vehicle, and (most critically) during deployment, and also during preflight sail checkout operations as well. Alternately, these secondary functions can, in general, be performed by the conventional ACS of a spacecraft bus; however, such systems would be significantly more massive. But the control offered by standard-size conventional ACS during sail deployment would not be robust to variations in symmetry during deployment. Micro-PPT technology enables a tremendous gain in sailcraft performance, most critically in the areas of agility, mass, and redundancy [18–20].

An overview of the state-of-the-art PPT technology, PPT performance requirements for solar sails, and the pulse-modulated PPT control design and simulation is presented in this section.

A. Recent Advances in Micro-PPT Technology

The purposes of this section are to provide a brief overview of the recent advances in micro-PPT technology applicable to solar-sail attitude control and to establish the foundation for developing the micro-PPT design requirements for solar sails.

A variety of microthrusters for stationkeeping and attitude control of microsatellites have been developed by NASA John H. Glenn Research Center, U.S. Air Force Research Laboratory (AFRL), Jet Propulsion Laboratory, and industry [21–25]. They include: the vaporizing liquid microthruster, the micron-sized cold-gas thruster, the micro-Hall thruster, the microion engine, the micropulsed plasma thruster, the free molecule microresistojet, and the digital microthruster array. Most of these microthrusters have an inherent

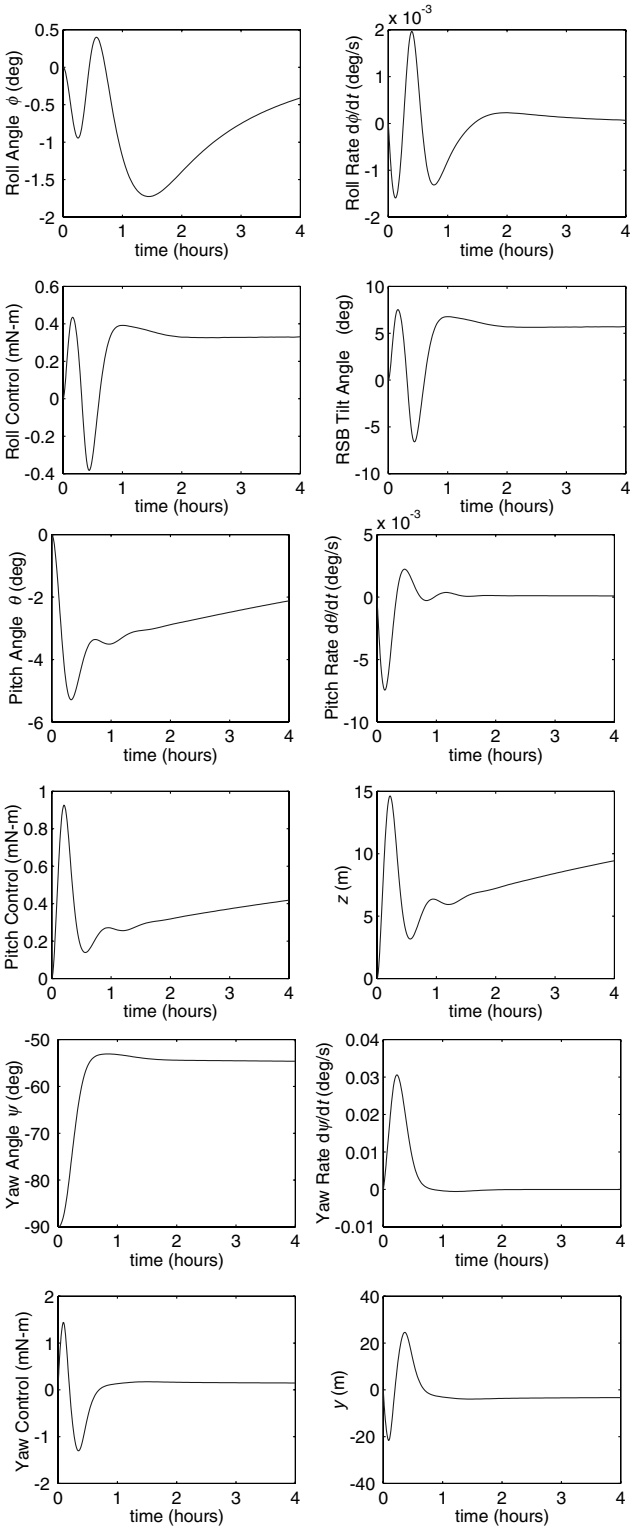

Fig. 12 A TVC mode simulation for an 8 km/day orbit raise ($\phi_c = \theta_c = 0$ deg and $\psi_c = -55$ deg).

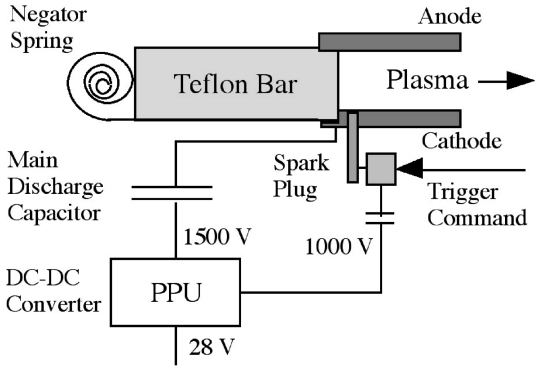

Fig. 13 Schematic of a pulsed plasma thruster.

problem of low specific impulse and/or low efficiency. However, such a low-I_{sp} and/or low-efficiency drawback of microthrusters may not be of significant importance for solar-sail attitude control applications, whereas other factors such as low thrust, low power, low mass, low volume, low voltage, and low impulse bit are more important. Among these microthrusters, a micro-PPT is judged most suitable for solar-sail attitude control applications because of its inherent simplicity (not requiring propellant tanks, micromachined valves, and complex feed systems) and its use of a solid Teflon propellant [21–25]. However, the spacecraft contamination issues involved with using Teflon propellant need to be further examined, and the selection of a particular type of attitude control propulsion system for a given mission is, in general, a complex problem, and it is strongly mission-dependent.

The PPT uses electric power to ionize and electromagnetically accelerate a plasma to high exhaust velocities. As illustrated schematically in Fig. 13, the PPT consists of a Teflon fuel bar, a negator spring, a power processing unit, capacitors, electrodes, a spark plug, and a trigger circuit. The main discharge, ignited by the spark plug, ablates and ionizes a small amount of Teflon from the face of the fuel bar into a plasma slug. The interaction of the current and the self-imposed magnetic field generates the $\boldsymbol{j} \times \boldsymbol{B}$ Lorentz force, which accelerates the plasma to high exhaust velocities.

The PPT technology has a long history of reliable space flight operation: for example, Russian Zond-2 Mars Probe in 1964, LES-6 spacecraft (by MIT Lincoln Laboratory) in 1968, LES-8/9 satellites, and NOVA satellites in the early 1980s [21]. Recently, several miniaturized PPTs have been developed for a variety of satellite applications. For example, a 5-kg PPT module by Primex Aerospace (now Aerojet-Redmond Operation) was flight validated on the EO-1 New Millennium Program mission [22]. A precision pitch attitude pointing capability of a PPT-based ACS was demonstrated for the EO-1 spacecraft while meeting stringent electromagnetic and contamination constraints. A 1-kg PPT module was also recently developed for the Dawgstar microsatellite [23,24]. Although the Dawgstar satellite did not become part of an actual flight program, a flight-qualified unit of such a 1-kg PPT module has been developed for use in microsatellites [24]. A much smaller 0.1-kg PPT unit was developed by the AFRL [25]. The 10-μN microPPTs by the AFRL were originally planned to fly on the TechSat21 mission as a technology demonstration, but they were never flown due to program cancellation of the TechSat21 mission. Such a significant miniaturization was made possible by using a self-igniting discharge, thus eliminating the separate igniter circuit from a standard PPT. Busek Corporation has taken over commercial development of the micro-PPT design from the AFRL and is providing microPPTs for the FalconSat3 program at the U.S. Air Force Academy. FalconSat3 is a 50-kg, 0.46-m cube microsatellite scheduled for launch in 2006 using the EELV/ESPA. Among its other mission objectives, FalconSat3 will demonstrate a micropropulsion attitude control system (MPACS) technology. A micro-PPT module is also installed at the end of a gravity-gradient boom. Each module of a total mass of 1.6 kg includes three thrusters, a shared main capacitor, and individual triggering units for each thruster with an impulse bit of 100 μN · s. The overall characteristics of these recently developed microPPTs are compared in Table 3.

Table 3 Comparison of recently developed micro-PPT modules

Parameter	EO-1	Dawgstar	AFRL	FalconSat3
Thrust,[a] μN	860	120	10	100[d]
Thrusters per module	2	2	1	3
Pulsing freqency, Hz	1	2	1	2
Impulse bit, μN · s	90–860	60	10	50[d]
Pulse energy, J	8.5–56	5	6.6	2
Total mass, kg	4.9	1	0.1	1.6
Power, W	70	15	1	8
I_{sp}, s	650–1350	242	——	——
Efficiency,[b] %	9.8	1.8	——	——
Total impulse,[c] N · s	925	140	——	——
Propellant,[c] kg	0.07	0.03	——	——

[a]Maximum steady thrust at maximum pulsing frequency.
[b]Thruster efficiency, not including the PPU efficiency.
[c]Per thruster.
[d]Beginning of life (BOL). Possibly, 50 at end of life (EOL).

Table 4 Design requirements for a 150-μN PPT

Sail size, m	40	80
Mast length, m	28	56
cm/cp offset,[a] m	0.1	0.2
Solar disturbance torque,[a] mN · m	1	8
Control torque,[b] mN · m	4.2	8.4[c]
Total impulse (required),[d] μN · s	1126	4505
Total pulses (required)[d]	7.5×10^6	30×10^6

[a]The normally worst case for untrimmed sailcraft.
[b]Using one thruster.
[c]This control torque can be doubled using a pair of thrusters.
[d]Per year.

B. PPT Requirements for Solar-Sail Attitude Control

As illustrated in Table 4, a thrust level of 150 μN is selected for use with a 40-m untrimmed sailcraft with large torque margins (and also for a larger sailcraft up to 80 m but with smaller torque margins). A pair of thrusters can also be employed to further increase control torque margins. It can be noticed that the EO-1 PPT module with a total mass of 4.9 kg is too heavy and the thrust level of AFRL's μPPT is too low to be employed for 150-kg class sailcraft. The Dawgstar PPT module with a total mass of 1 kg has a thrust level of 120 μN (at 2 Hz pulsing frequency), but its current design has a total impulse of only 140 N · s (per thruster), which is too small for solar-sail attitude control applications.

Consequently, a prototype lightweight PPT module, named PPT150, has been being developed for use in solar-sail attitude control by employing the design methodology of the flight-proven

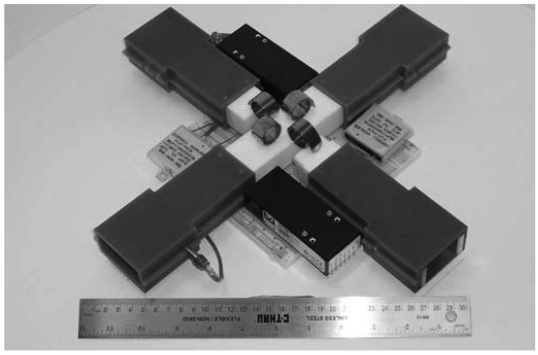

Fig. 14 A 150-μN, 15-W, 2-kg micro-PPT module currently under preliminary development and testing for solar-sail attitude control applications (preassembled for the purpose of illustrating its overall cross-axis configuration and components) [18–20].

Table 5 Design parameters of the PPT150 module for solar-sail attitude control

Parameter	Value
Total mass	2 kg
Thrusters	4
Impulse bit	150 μN · s
Pulse frequency (max)	1 Hz
Steady thrust (max)[a]	150 μN
Pulse energy	15 J
Peak power[a]	20 W
Average power[a]	15 W
I_{sp}	500 s
Efficiency	5 %
Total impulse[a]	1500 N · s
Propellant[a]	0.2 kg

[a]Per a single thruster unit.

EO-1 PPT module. As shown in Fig. 14, the PPT150 module has four thruster units. Preliminary design characteristics of the PPT150 module are summarized in Table 5. Similar to mounting control vanes at the mast tips, four PPT modules will be mounted at the mast tips, as illustrated in Fig. 15, to use the largest moment arm length. A yaw-axis dynamic model with tip-mounted micro-PPTs and a translating control mass are also illustrated in Fig. 16. A mast tip-mounted PPT150 of a maximum steady thrust level of 150 μN (at 1 Hz pulsing frequency) provides a maximum control torque of 4.2 mN · m for a 40-m sailcraft (using a single thruster).

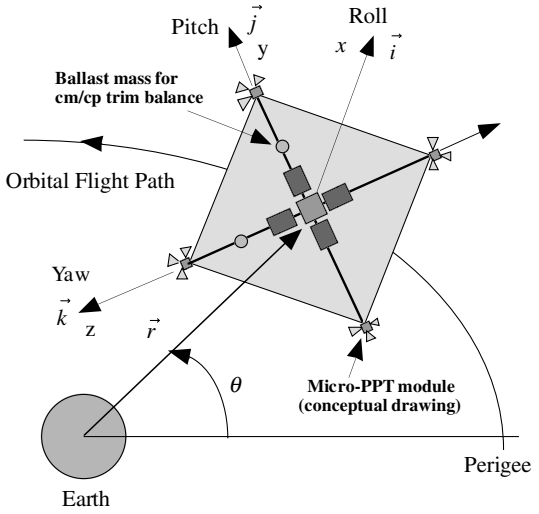

Fig. 15 Sailcraft equipped with a propellantless primary ACS and a micro-PPT-based secondary ACS.

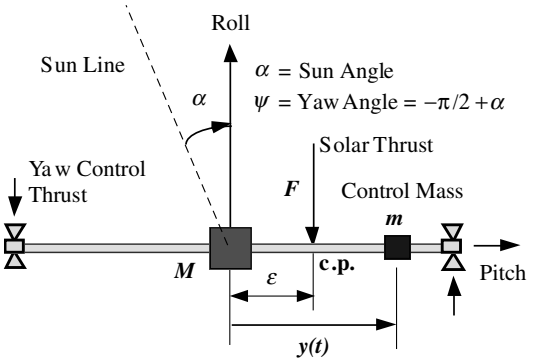

Fig. 16 Yaw-axis dynamic model with tip-mounted micro-PPTs and a moving control mass.

C. Pulse-Modulated On-Off Control Using Micro-PPTs

Pulse modulation represents the common control logic behind most reaction-jet control systems of spacecraft. Unlike other actuators, such as reaction wheels, thruster output consists of two values: on or off. Proportional thrusters, whose fuel valves open a distance proportional to the commanded thrust level, are not often employed in practice. Mechanical considerations prohibit proportional valve operation largely because of dirt particles which prevent complete closure for small valve openings; fuel leakage through the valves consequently produces opposing thruster firings. In general, pulse modulators produce a pulse command sequence to the thruster valves by adjusting the pulse width and/or pulse frequency [10].

The pulse width modulator (PWM) shown in Fig. 17 differs from other modulators, such as a pulse width and pulse frequency (PWPF) modulator, that it is essentially a discrete-time device. The PWPF modulator can be digitally implemented but is often analyzed as a continuous-time system. The output of a PWM is not a thruster-firing state; instead, the PWM output is thruster pulse width, as illustrated in Fig. 18.

A single-axis control loop design model of a reaction-jet control system with a PWM is illustrated in Fig. 17. The value d_1 represents the minimum pulse width of the system; this deadzone is directly proportional to the attitude deadband. The value d_2 represents the

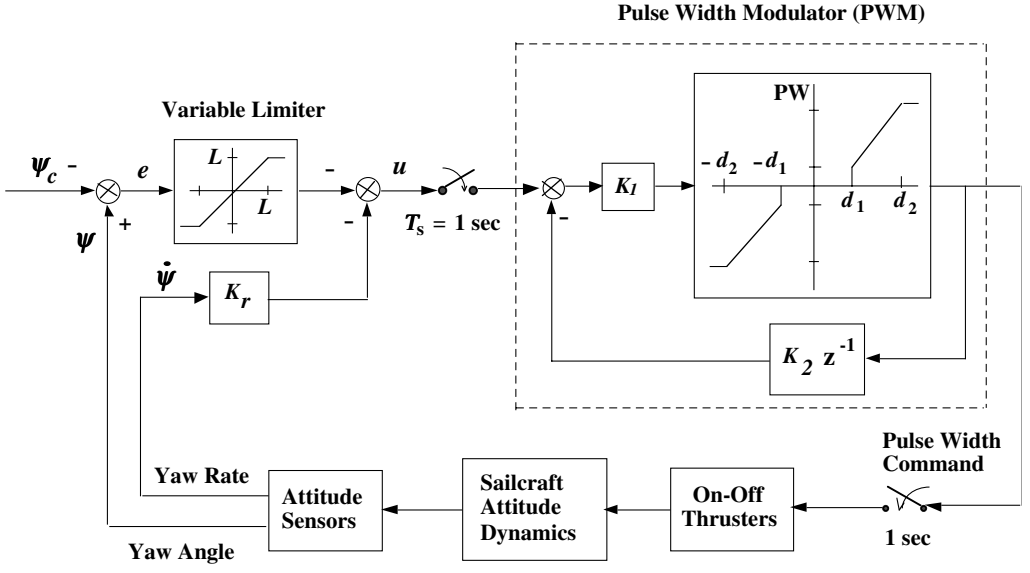

Fig. 17 Single-axis control loop design model of a microthruster-based sail ACS.

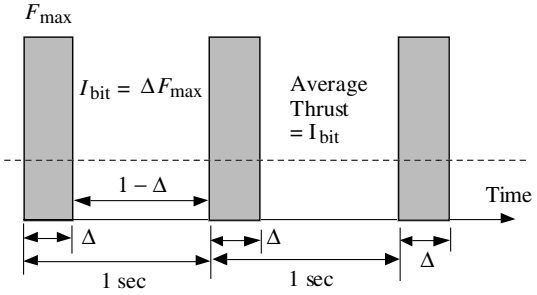

Fig. 18 Steady-state pulse firings of a PPT at 1-Hz pulse frequency.

maximum pulse width of a thruster; it is often chosen to be the digital control sampling period. The delay in the feedback loop introduces damping to the system; maximum damping occurs when the feedback signal is smaller than the PWM input. If the input signal is not greater than the feedback signal, the modulator may limit cycle itself. This criterion enables the designer to determine the feedback gain K_2. The feedforward gain K_1 is selected as result of the minimum pulse width and the attitude deadband. More details of pulse modulation techniques as applied to spacecraft attitude control systems design can be found in [10].

As illustrated in Fig. 17 for the yaw axis, the pulse control logic is given by

$$u = -\{\underset{L}{\text{sat}}(e) + K_r\dot{\psi}\} \tag{42}$$

where

$$e = \psi - \psi_c \tag{43}$$

$$L = K_r \min\{\sqrt{2a|e|}, \omega_{\max}\} \tag{44}$$

For a PPT with a fixed impulse bit, I_{bit} and a maximum pulsing frequency of 1 Hz, as illustrated in Fig. 18, we simply choose $K_1 = 1$, $K_2 = 0$, and $d_1 = d_2$. A single pulse firing is commanded if $|u| > d_1$ where d_1 is the desired attitude deadband. Preliminary design values of the PPT-based ACS are provided in Table 6.

The feasibility of controlling a 40-m untrimmed sailcraft in a 1600-km DDSS orbit using the proposed micro-PPT-based ACS is demonstrated in Fig. 19, using three-axis coupled dynamic simulation in the presence of orbital as well as solar pressure disturbances. In Fig. 19, an attitude recovery maneuver for achieving the LVLH orientation of the zero-thrust mode was simulated. The initial tumbling conditions were: $\phi(0) = \theta(0) = 20$ deg, $\psi(0) = 90$ deg, and $\dot{\phi}(0) = \dot{\theta}(0) = \dot{\psi}(0) = 0.05$ deg/s. As demonstrated in this simulation, the proposed micro-PPT-based ACS provides a backup control capability for achieving the zero-thrust safe mode with $\psi(0) = 0$ deg.

Table 6 Preliminary design of a micro-PPT-based ACS for a 40-m sailcraft

Parameter	Value
Sampling time T_s	1 s
Pulsing freqency (max)	1 Hz
I_{bit}	150 μN · s
Δ	15 μs
F_{max}	10 N
Average thrust (max)	150 μN
Average torque (max)	4.2 mN · m
d_1	0.002 rad
d_2	0.002 rad
Attitude deadband	$\pm$0.1 deg
K_1	1
K_2	0
K_r	300 rad^{-1}
ω_{max}	0.05 deg/s

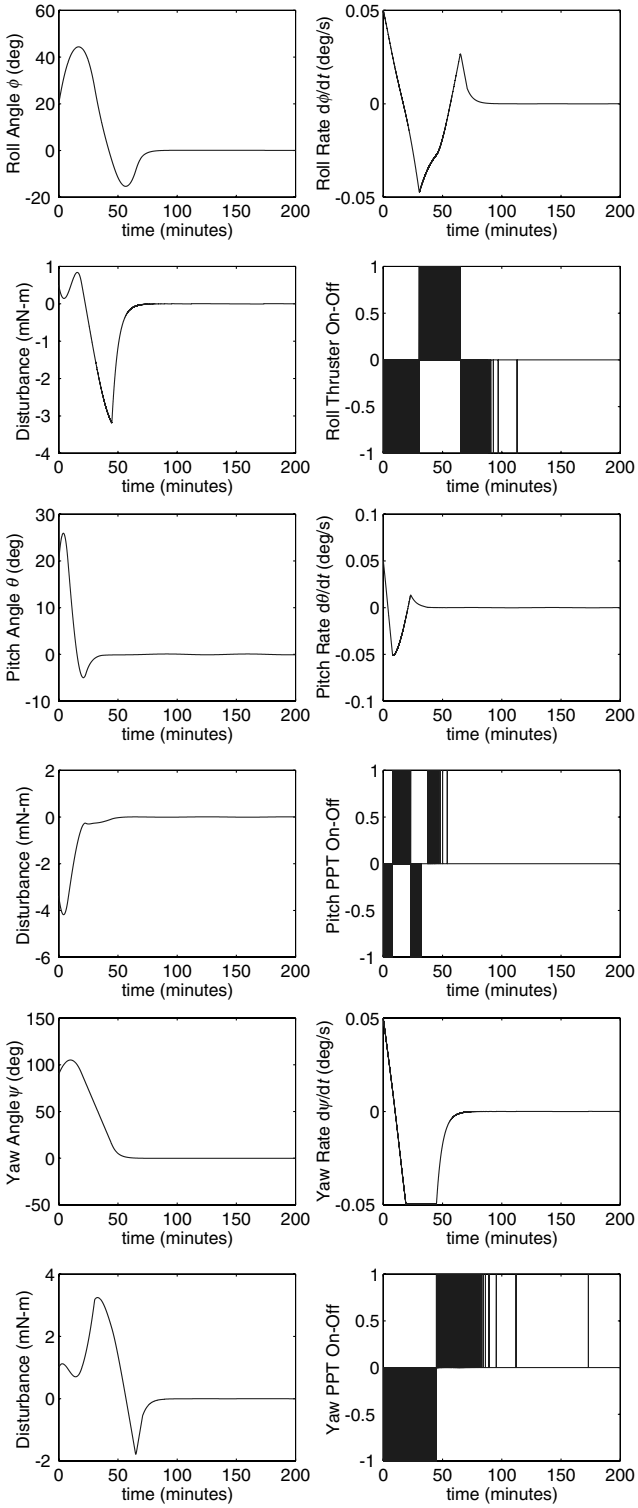

Fig. 19 Attitude recovery maneuver using the PPT-based ACS for an untrimmed sailcraft in a 1600-km DDSS orbit ($\phi_c = \theta_c = \psi_c = 0$ deg).

VII. Conclusions

A solar-sail ACS architecture has been developed for a solar-sail flight validation experiment of a 40-m, 150-kg solar-sail spacecraft in a 1600-km DDSS orbit. The numerous advantages of the DDSS orbit over an elliptical transfer orbit such as a geosynchronous transfer orbit or supersynchronous transfer orbit have also been demonstrated for a near-term, low-risk flight-validation experiment. The proposed solar-sail ACS architecture will be applicable with minimal modifications to a wide range of future solar-sail flight missions with varying requirements and mission complexity.

Acknowledgments

The work described in this paper was funded by the In-Space Propulsion Technology Program, which is managed by NASA's Science Mission Directorate in Washington, DC, and implemented by the In-Space Propulsion Technology Office at Marshall Space Flight Center in Huntsville, Alabama. The program objective is to develop in-space propulsion technologies that can enable or benefit near and midterm NASA space science missions by significantly reducing cost, mass, or travel times. The author would like to thank E. Montgomery, G. Garbe, J. Presson, A. Heaton, and M. Whorton at NASA Marshall Space Flight Center for their financial and technical support.

References

[1] McInnes, C. R., *Solar Sailing: Technology, Dynamics and Mission Applications*, Springer Praxis Publishing, Chichester, U.K., 1999.

[2] Garbe, G., and Montgomery, E., "An Overview of NASA's Solar Sail Propulsion Project," AIAA Paper 2003-4662, July 2003.

[3] Murphy, D. M., Murphey, T. W., and Gierow, P. A., "Scalable Solar Sail Subsystem Design Concept," *Journal of Spacecraft and Rockets*, Vol. 40, No. 4, 2003, pp. 539–547.

[4] Murphy, D. M., McEachen, M. E., Macy, B. D., and Gaspar, J. L., "Demonstration of a 20-m Solar Sail System," AIAA Paper 2005-2126, April 2005.

[5] Wright, J. L., *Space Sailing*, Gordon and Breach, New York, 1992.

[6] Murphy, D., and Wie, B., "Robust Thrust Control Authority for a Scalable Sailcraft," AAS Paper 04-285, Feb. 2004.

[7] Wie, B., "Solar Sail Attitude Control and Dynamics: Parts 1 and 2," *Journal of Guidance, Control, and Dynamics*, Vol. 27, No. 4, 2004, pp. 526–544.

[8] Brady, T., Tillier, C., Brown, R., Jimenez, A., and Kourepenis, A., "The Inertial Stellar Compass: A New Direction in Spacecraft Attitude Determination," SSC Paper 02-II-1, Aug. 2002.

[9] Lappas, V., and Wie, B., "Advanced Small Satellite Bus Technology for Near-Term Solar Sail Missions," AIAA Paper 2006-6179, Aug. 2006.

[10] Wie, B., *Space Vehicle Dynamics and Control*, AIAA Education Series, AIAA, Washington, DC, 1998, pp. 36–40, 365–374, 451–456.

[11] Kaplan, M., *Modern Spacecraft Dynamics and Control*, John Wiley & Sons, New York, 1976, pp. 379–394.

[12] Wie, B., and Lu, J., "Feedback Control Logic for Spacecraft Eigenaxis Rotations Under Slew Rate and Control Constraints," *Journal of Guidance, Control, and Dynamics*, Vol. 18, No. 6, 1995, pp. 1372–1379.

[13] Wie, B., Heiberg, C., and Bailey, D., "Rapid Multi-Target Acquisition and Pointing Control of Agile Spacecraft," *Journal of Guidance, Control, and Dynamics*, Vol. 25, No. 1, 2002, pp. 271–282.

[14] Wie, B., Murphy, D., Thomas, S., and Paluszek, M., "Robust Attitude Control Systems Design for Solar Sail Spacecraft (Part 1): Propellantless Primary ACS," AIAA Paper 2004-5010, Aug. 2004.

[15] Thomas, S., Paluszek, M., Wie, B., and Murphy, D., "Design and Simulation of Sailcraft Attitude Control Systems Using Solar Sail Control Toolbox," AIAA Paper 2004-4890, Aug. 2004.

[16] Wie, B., Thomas, S., Paluszek, M., and Murphy, D., "Propellantless AOCS Design for a 160-m, 450-kg Solar Sail Spacecraft of the Solar Polar Imager Mission," AIAA Paper 2005-3928, July 2005.

[17] Wie, B., "Thrust Vector Control Analysis and Design for Solar Sail Spacecraft," *Journal of Spacecraft and Rockets* (to be published).

[18] Pryor, K., Wie, B., and Mikellides, P., "Development of a Lightweight Pulsed Plasma Thruster Module for Solar Sail Attitude Control," SSC Paper 04-XI-4, Aug. 2004.

[19] Wie, B., Murphy, D., Thomas, S., and Paluszek, M., "Robust Attitude Control Systems Design for Solar Sail Spacecraft (Part 2): MicroPPT-Based Backup ACS," AIAA Paper 2004-5011, Aug. 2004.

[20] Wie, B., and Murphy, D., "MicroPPT-Based Secondary/Backup ACS for a 160-m, 450-kg Solar Sail Spacecraft," AIAA Paper 2005-3724, July 2005.

[21] Micci, M., and Ketsdever, A. (eds.), *Micropropulsion for Small Spacecraft*, Vol. 187, Progress in Astronautics and Aeronautics, AIAA, Washington, DC, 2000, Chap. 3.

[22] Benson, S., Arrington, L., Hoskins, A., and Meckel, N., "Development of a PPT for the EO-1 Spacecraft," AIAA Paper 99-2276, June 1999.

[23] Cassady, R., Hoskins, A., Campbell, M., and Rayburn, C., "A Micro Pulsed Plasma Thruster (PPT) for the Dawgstar Spacecraft," *Proceedings of the 2000 IEEE Aerospace Conference*, Vol. 4, IEEE Press, Piscataway, NJ, 2000, pp. 7–14.

[24] Rayburn, C., Campbell, M., and Mattick, A., "Pulsed Plasma Thruster System for Microsatellites," *Journal of Spacecraft and Rockets*, Vol. 42, No. 1, 2005, pp. 161–170.

[25] Spanjers, G., Bromaghim, D., Lake, J., Dulligan, M., White, D., Schilling, J., Bushman, S., Antonsen, E., Burton, R., Keidar, M., and Boyd, I., "AFRL MicroPPT Development for Small Spacecraft Propulsion," AIAA Paper 2002-3974, July 2002.

R. Braun
Associate Editor